Confinement-Induced Morphologies of Cylinder-Forming Asymmetric Diblock Copolymers

Bin Yu,[†] Qinghua Jin,[†] Datong Ding,*[,†] Baohui Li,*[,†] and An-Chang Shi*[,‡]

College of Physics and Key Laboratory of Functional Polymer Materials of Ministry of Education, Nankai University, Tianjin, 300071, China, and Department of Physics and Astronomy, McMaster University, Hamilton, Ontario L8S 4M1, Canada

Received November 2, 2007; Revised Manuscript Received March 21, 2008

ABSTRACT: Self-assembly of cylinder-forming diblock copolymers confined in cylindrical nanopores is studied systematically using a simulated annealing method. The diblock copolymers form hexagonally packed cylinders in the bulk with a period L_0, whereas novel structures spontaneously form when the copolymers are confined inside cylindrical pores. It is discovered that the sequence of structures is controlled by the ratio between the pore diameter (D) and L_0, as well as the selectivity of the pores. For selective small pores ($D/L_0 < 2.7$), the following structural sequence occurs as the pore size is increased: a string of spheres, a single cylinder, a straight band, a twisted band or stacked disks, a single helix, a set of degenerate structures (includes single helix, stacked toroids and double helices), and double helices. For larger pores ($D/L_0 > 2.7$), the outer ring of the minority block-domain forms helices or stacked toroids, while the inner structure repeat the sequence of structures observed in smaller pores. For neutral pores, cylinders oriented parallel and nearly perpendicular to the cylindrical pore are observed besides helical or toroidal structures. These morphologies are consistent with available experiments and theoretical studies. Mechanisms of the morphological transitions can be understood based on the degree of commensurability between the pore diameter and bulk period of the copolymer L_0, parametrized by the ratio D/L_0. The effect of the cylindrical pore length on final morphologies is investigated. The chain conformations as a function of morphologies are calculated and analyzed. A mechanism for the formation of helices is proposed based on a packing model, which gives a reasonable description of the radius and pitch of the observed helices.

Introduction

The self-assembled structures of block copolymers have attracted tremendous scientific interests in the last dacades.[1,2] For the simplest block copolymers, i.e., A−B diblock copolymers, the self-assembled structures include a body centered-cubic array of spheres, hexagonally packed cylinders, lamellae, and a bicontinuous gyroid structure, as have been observed experimentally and theoretically.[3,4] The mesoscopic structures of block copolymers possess a great potential for technological applications. Therefore, it is desirable to develop different routes of engineering new block copolymer structures. Besides using more complex block copolymers to produce new structures, external degrees of freedom, such as applied fields or geometric confinements, are possible routes to induce new structures. Recently diblock copolymers under confinement have attracted considerable attention[5] due to their rich phase behavior[6] and their possible technological applications in diverse areas such as templating in lithographic processes,[7] optical devices,[8] and surfaces with molecular recognition capabilities.[9] In geometrically confined block copolymer systems, molecular organization can be strongly influenced by the commensurability between the physical dimension of the confinement and the bulk period of the copolymer, confinement-induced entropy loss, and surface interactions. Previously reported studies of confinement effects[10,11] have focused on lamella-forming block copolymers in one-dimensional confinements. For example, for symmetric diblock-copolymer films sandwiched between two flat surfaces, when the film thickness is incommensurate with the bulk lamellar period, the lamellae parallel to the surfaces will be forced to assume a different thickness.[11] This change of period will lead to an increase of free energy of the copolymers, leading to the possibility of reorganization of the structures. Asymmetric diblock copolymers under one-dimensional confinement have also been studied though with much less attention.[12−15] As in the case of lamella-forming diblock copolymers, the interplay between confinement and preferential interfacial interactions cause deviations from the morphology observed in the bulk.

Two-dimensional confinements in the form of cylindrical pores present a more tightly confined geometry as compared with thin films. It is expected that two-dimensional confinements may lead to richer phase behaviors. Indeed the complexity of two-dimensionally confined diblock copolymers has been demonstrated recently. In a Monte Carlo simulation study, He et al.[16] investigated the morphologies of lamella-forming diblock copolymer melts confined in cylindrical pores which are selective for one of the blocks. Circular lamellae parallel to the pore wall have been identified. Using dynamical density functional simulations, Sevink et al.[17] identified stacked disks, i.e., lamellae perpendicular to the pore axis for neutral walls, as well as circular lamellae parallel to the pore surface for a strong selective wall for one of the blocks. In further Monte Carlo simulations, Chen et al.,[18] Feng et al.,[19] Wang,[20] and Yu et al.[21] have identified other morphologies, such as porous lamellar (mesh) morphologies, lamellae parallel to the pore axis, as well as single and double helices, for lamella-forming diblock copolymer melts confined in cylindrical pores. Using dissipative particle dynamics (DPD) simulations, Feng et al. have also identified similar morphologies for lamella-forming diblock copolymer melts confined in cylindrical pores.[22] Experimentally, Russell and co-workers discovered that for the lamella-forming symmetric polystyrene-*b*-polybutadiene (PS-*b*-PBD) diblock copolymers confined within nanoscopic cylindrical pores in alumina membranes,[23−25] a multiple set of circular lamellae parallel to the pore surface is observed when the pore diameter (D) is larger than the equilibrium period L_0. Circular lamellar structures have also been observed by Sun and co-workers in

* To whom correspondence should be addressed. E-mail: baohui@nankai.edu.cn; shi@mcmaster.ca.
[†] College of Physics and Key Laboratory of Functional Polymer Materials of Ministry of Education, Nankai University.
[‡] Department of Physics and Astronomy, McMaster University.

10.1021/ma702430v CCC: $40.75
Published on Web 05/09/2008

the study of symmetric polystyrene-*b*-poly (methyl methacrylate) diblock copolymers confined in alumina nanopores,[26] and by Ma and co-workers in the study of styrene-isoprene block copolymers nanowires.[27] Russell and co-workers have also observed a novel toroid morphology in their study of symmetric lamella-forming PS-*b*-PBD diblock copolymers under similar confinement,[24,25] which occurs when the pore diameter D is comparable to L_0 and D/L_0 is not an integer. In a series of papers, Russell and co-workers reported the study of asymmetric (cylinder- and sphere-forming) PS-*b*-PBD diblock copolymers confined in alumina nanopores.[23,25,28] For cylinder-forming PS-*b*-PBD, they observed that large pores ($D/L_0 > 4.1$) lead to hexagonally packed cylindrical domains, the symmetry and domain spacing of the cylinders can be altered by the shape and size of the pores. On the other hand, in nanopores with smaller diameters ($D/L_0 = 1.1-1.5$), the morphology has changed from simple cylinders oriented parallel to the pores to a structure in which the cylinders form helices within the pores.[28] For sphere-forming PS-*b*-PBD, they observed that large pores ($D/L_0 > 3.2$) lead to spherical PBD domains aligned along the pore axis, whereas in pores with smaller diameters ($D/L_0 < 3.2$), helical arrays of spheres are observed.[25] Theoretically, Li and co-workers[29,30] and Chen and co-workers[31] have carried out self-consistent field theory (SCFT) calculations for diblock copolymers under circular confinement. They discovered a rich variety of new structures, including the experimentally observed straight cylindrical, circular lamellar domains, and helical structures. With simulations, Feng and co-workers[19] and Feng and co-workers[22] also discovered helical structures for asymmetric diblock copolymer melts confined in cylindrical pores. In a related work, Wu et al. studied the confined assembly of silica−surfactant composite mesostructures within cylindrical nanopores of varying diameters.[32] They observed that the cylinder-forming systems under this two-dimensional confinement spontaneously form unusual silica structures such as helices and toroids. Furthermore, they have carried out SCFT calculations on a model system composed of diblock-copolymer and homopolymer blends. The SCFT results are used to account for the observed coassembled mesostructures. All these previous studies demonstrated the possibility that confinement can lead to unusual morphologies that are not accessible in the bulk, thus providing opportunities to engineer novel structures.

Motivated by these previous experimental and theoretical studies, we have carried out a systematic study of cylinder-forming diblock copolymers confined in the cylindrical pores. The equilibrium morphologies are obtained as a function of the degree of confinement and surface interactions of the cylindrical pores. It has been discovered that novel structures, such as helices and stacked toroids, spontaneously form inside the cylindrical pores. A brief communication of our studies on cylinder-forming diblock copolymers confined in cylindrical pores has been published in a short letter.[33] The purpose of the present paper is two-fold. First of all, the current paper gives a detailed account of the studies along with some unpublished new results. In particular, details of the algorithm and results are given. Refined boundaries between different morphologies are obtained. The effect of the cylindrical pore length on final morphologies is invistigated. The chain conformations in all obtained structures are analyzed. The second purpose of the current paper is to present an understanding of the mechanism for the formation of the novel structures. In particular, a simple model is proposed to account for the formation of helices. The radius and the pitch of the equilibrium helical structures are computed and compared with the simple model predictions.

Model and Methods

In our studies, the equilibrium structures are explored using computer simulations on a lattice model of polymers. The computer simulation studies were based on a simulated annealing method,[34] which is a well-known procedure for obtaining the lowest-energy "ground states" in disordered systems.[35,36] The polymers are modeled using the "single-site bond fluctuation" model, which was proposed by Carmesin and Kremer[37] and by Larson.[38] Specifically, cylinder-forming model diblock copolymers of the form A_n-*b*-B_{N-n} are used in the study, where $N = 12$, and $n = 2$ and 3. The volume fraction of the A-blocks is $f_A = 1/4$ and $f_A = 1/6$, respectively, for these two model diblock copolymers. The interaction of the A-B monomers is modeled using a nearest-neighbor interaction energy $\varepsilon_{AB} = 1.0k_BT_{ref}$, where k_B is the Boltzmann constant and T_{ref} is a reference temperature. Simulations are performed for these block copolymers in bulk and confined in long cylindrical pores. For all the simulations, the model system is embedded in a simple cubic lattice of volume $V = L_x \times L_y \times L_z$. For bulk phases, periodic boundary conditions are used in all three directions. For confined simulations, the pore axis is along the z direction along which periodic boundary condition is applied. L_x and L_y are equal and chosen to be at least 2 lattice spaces larger than the pore diameter D.[33] The pore axis consists of the central lattice site in each $x-y$ plane, and the pore consists of all the lattice sites with a distance to the pore axis not larger than $D/2$. Lattice sites outside the pore constitute the pore-wall. Polymers cannot occupy the wall sites, therefore they are confined to a long cylindrical pore of diameter D. Depending on the interactions between pore-wall and polymer, three types of the pores are considered: (1) the pore is strongly attractive to the majority blocks ($\varepsilon_{WA} > \varepsilon_{WB}$), (2) the pore is strongly attractive to the minority block ($\varepsilon_{WA} < \varepsilon_{WB}$), and (3) the pore is neutral ($\varepsilon_{WA} = \varepsilon_{WB}$).

The starting configuration of the current study is slightly different from that used in our previous communication.[33] The initial state is generated by putting an array of copolymer chains onto the lattice. The polymer chains are parallel to one of the lattice axis. These chains are either in an extended or one-fold conformation. This is different from our previous study,[33] where all the polymer chains in the initial state are extended. First, a maximum concentration of monomers is generated (in all case the maximum concentration is higher than 95%) by inserting polymer chains sequentially. Randomly chosen chains are then removed from the box until the desired concentration (85%) is reached. After the desired number of chains has been taken out, the remaining empty sites were assigned to vacancies. Starting from the initial state, the ground-state of the system is obtained by executing a set of Monte Carlo simulations at decreasing temperatures. Our results show that the starting configuration has a negligible influence on the final morphology in most cases. On the other hand, some final morphology for cylindrical pores with large diameters can be influenced by the initial configurations. Two types of trial moves are used in the simulations, which are the same as those used in our previous studies.[15,21,39] Specifically these trial moves are as follows. (1) Chain reverse: A chain is selected, and all the A monomers on the chain are exchanged with the B monomers on the same chain. (2) Exchange movements: A vacancy is selected, and it can exchange with a monomer on one of its 18 nearest neighbors. If the exchange does not break the chain, it is allowed. If the exchange creates a single break in the chain, the vacancy will continue to exchange with subsequent monomers along the chain until reconnection of the links occurs. If the exchange breaks the chain in two chains, it is not allowed. The acceptance or rejection of the attempted moves is further governed by the Metropolis rule.[40]

The annealing procedure followed the usual linear annealing schedule, $T_j = fT_{j-1}$, where T_j is the temperature used in the jth annealing step and f is a scaling factor. The annealing was continued until the temperature reached a predetermined value (T_M). In our simulations, $T_1 = 30T_{ref}$, the temperature T reaches T_M ($=T_{70}$) after 70 annealing steps. The scaling factor f was taken to be 0.92 or 0.95, depending on the difference of the average energies of the

system at the previous two annealing steps. $f = 0.92$ was used when the difference of the average energy is small, and $f = 0.95$ was used when the average energy difference is large. One Monte Carlo step (MCS) is defined as the time for, on average, all the chains to be reversed and all the lattice sites to be visited one time. At each annealing step, 25 000 MCS are performed.

Results and Discussions

Morphology of the Bulk System. We have reported that for the model diblock copolymers A_n-b-B_{N-n} with $N = 12$, hexagonally packed cylinders are formed for $f_A = {}^1/_4$ and $f_A = {}^1/_6$.[33] For these copolymers, simulation boxes with various sizes have been used. It is discovered that although hexagonally packed cylinders can be obtained for any box size, the orientation of the cylinders depends on the box size. In our simulations, the box size is adjusted such that the hexagonally packed cylinders are parallel to one of the lattice axis. The equilibrium spacing between the cylinders can then be calculated from the simulated equilibrium structures.

Specifically, L_z is fixed at $L_z = 24$, while L_x and L_y are varied according to the relationship $L_y \approx kL_{0p}$ and $L_x \approx \sqrt{3}(k-1)L_{0p}$. Here L_{0p} is an estimated equilibrium spacing between the cylinders and k is an integer which is larger or equal to 2. Under these conditions, it is observed that hexagonally packed cylinders parallel to the z-axis are formed at some specific L_x and L_y values. For the copolymers with $f_A = {}^1/_4$, when $L_x = 18$ and $L_y = 20-22$ the simulation box contains cylinders showing two periods, whereas when $L_x = 37$ and $L_y = 32$, the box contains cylinders showing three periods. For the copolymers with $f_A = {}^1/_6$, the corresponding box sizes are $L_x = 17-18$ and $L_y = 19-21$ for the two-period structure and $L_x = 34$ and $L_y = 30$ for the three-period structure, respectively. The equilibrium bulk morphologies for $f_A = {}^1/_4$ (with box size $37 \times 32 \times 24$) and for $f_A = {}^1/_6$ (with box size $34 \times 30 \times 24$) are shown in Figure 1. These plots are generated as iso-surface contour plots of the A-monomers and viewed along the cylindrical axis. It is obvious that very regular hexagonally packed cylinders are obtained in the bulk phases.

The equilibrium spacing between the cylinders shown in Figure 1 can be obtained by calculating the average distance between the cylinders along two lattice directions.[13] The equilibrium distances between the cylinders in Figure 1a are $32/3 \cong 10.667$ and $\sqrt{(37/4)^2 + (32/6)^2} \cong 10.677$ lattice spacings in the two directions, respectively. Similarly the cylinder-spacings in Figure 1b are $30/3 = 10.000$ and $\sqrt{(34/4)^2 + (30/6)^2} \cong 9.862$, respectively. It is comforting to observe that the difference between the two values of the equilibrium spacing in the two directions is very small, demonstrating the fact that the system has reached a structure of hexagonally packed cylinders. The average of the two values is taken as the bulk period, resulting in a bulk period of $L_0 = 10.67$ lattice spacing for $f_A = {}^1/_4$ and $L_0 = 9.93$ lattice spacing for $f_A = {}^1/_6$, respectively. Because hexagonally packed cylinders are incommensurate with the square lattice in the $x-y$ plane, the bulk period obtained here is an approximation. We can estimate the error by performing simulations with different box size. The simulations show that the orientation of the cylinders is not parallel to the z-axis when $L_y = 32 \pm 1$ for $f_A = {}^1/_4$ or $L_y = 30 \pm 1$ for $f_A = {}^1/_6$. From this observation we can conclude that the error is less than one lattice spacing in the y-direction. Cylinders with three periods are formed in the y-direction for these sizes (Figure 1), thus the error in the bulk period L_0 is less than ± 0.33 lattice spacing. Considering that the error is much smaller than L_0, we neglect its influence in the following discussions. Another important length scale for the cylindrical structures is the diameter of the cylinders, d. Assuming the system is at the strong segregation limit (SSL), the diameter of the self-assembled cylinders d can be estimated using the relation $d^2 = 2\sqrt{3}f_A L_0^2/\pi$. For the two cylinder-forming diblock copolymers with $f_A = {}^1/_4$ and $f_A = {}^1/_6$, the cylinder diameter is estimated as $d = 0.5250L_0$ and $d = 0.4286L_0$, respectively.

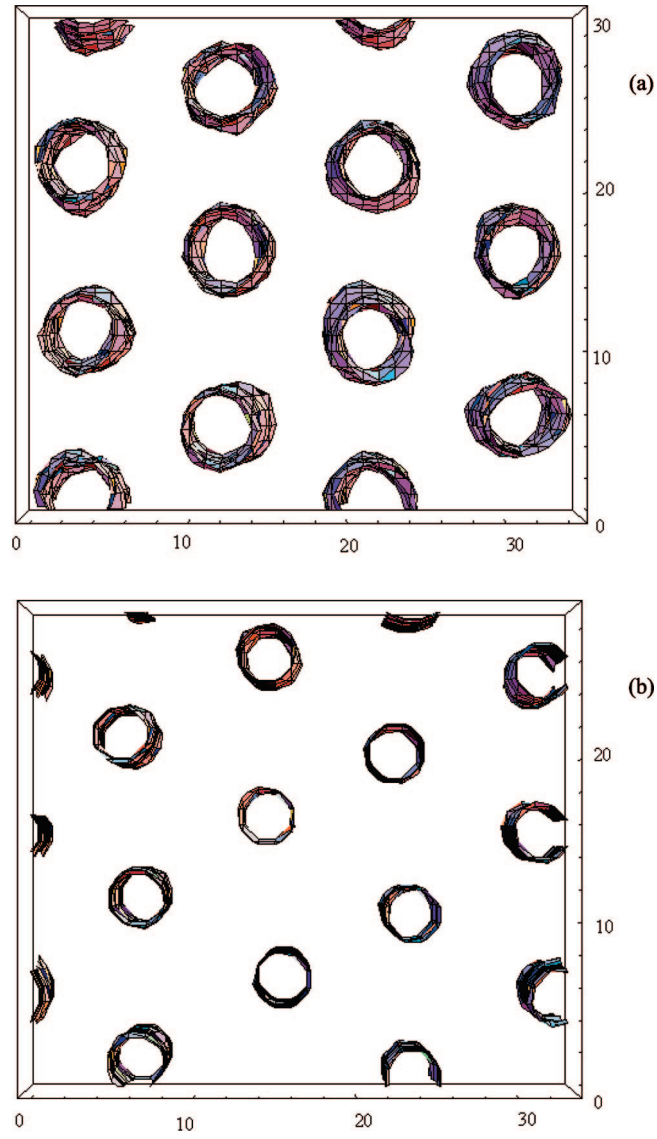

Figure 1. Self-assembled morphologies of the bulk systems. The cylinders are viewed along their axis. The z-direction, which is the axis of the cylinders, is perpendicular to the paper. (a) $f_A = {}^1/_4$ and the box size is $37 \times 32 \times 24$; (b) $f_A = {}^1/_6$ and the box size is $34 \times 30 \times 24$.

Morphologies of the Confined Systems. For simulations of the confined self-assembly, the cylinder-forming diblock copolymers with $f_A = {}^1/_4$ or $f_A = {}^1/_6$ are confined to a long cylindrical pore of diameter D. A systematic study of the confinement-induced structures is carried out with different pore diameters and pore−polymer interactions. In what follows results are presented for three typical cases, in which the pore wall is strongly attractive to the majority blocks (case 1), to the minority block (case 2), and neutral (case 3). It is observed that the equilibrium morphology of the confined system depends sensitively on the pore size and pore−polymer interactions. Typical self-assembled morphologies for different pore−polymer interactions are summarized in Figure 2. Since structural frustration is characterized by the ratio between the pore diameter and the spacing between the cylinders, the morphologies in Figure 2 are organized as a function of the ratio D/L_0. The morphologies are viewed from

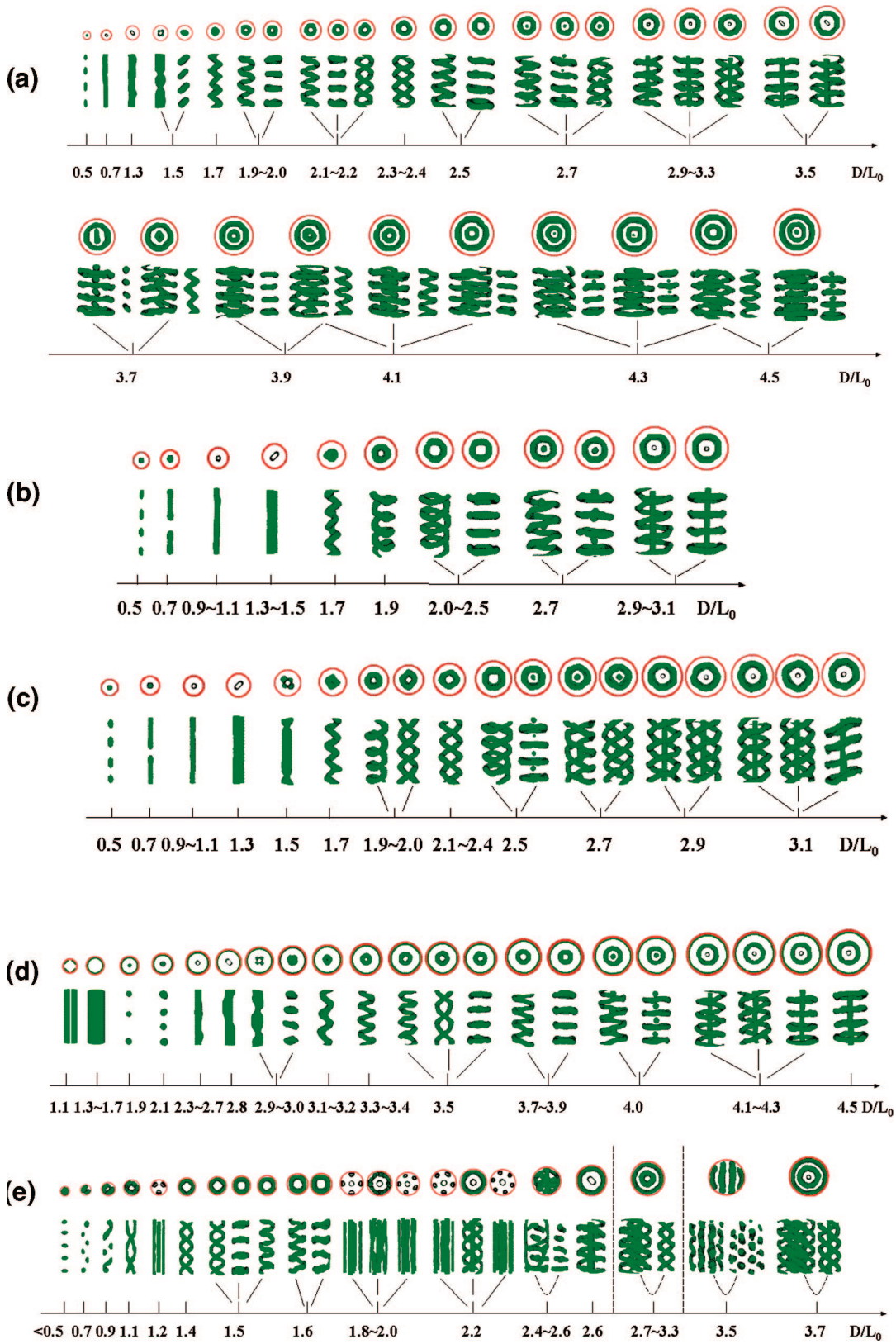

Figure 2. Self-assembled morphologies for the confined systems. The morphologies are organized as a function of the ratio D/L_0 for different wall-polymer interactions and different pore length. Both a top view and a side view are given. The outermost circles in the top views indicate the wall of the cylindrical pores. For some large diameters, the inner ring is shown separately. (a, b, and c) The case where the wall attracts the majority blocks (case 1): (a) $L_z = 40$, (b) $L_z = 38$, and (c) $L_z = 42$. (d) The case where the wall attracts the minority blocks (case 2), $L_z = 40$. (e) The case of a neutral wall (case 3).

both top and side of the pore. Although very similar morphologies have been presented previously,[33] Figure 2 contains a number of new results: (1) more detailed morphologies and morphological transition boundaries are given; (2) more regular morphologies are obtained for larger pores in the present paper due to the different starting configurations; (3) the effect of the

cylindrical pore length on final morphologies is investigated. The description of the overall morphology has been given in ref 33. Some details which were not described in our previous work[33] are presented in the rest of this section.

Case 1: $f_A = 1/6$, $\varepsilon_{WA} = 1.0k_BT_{ref}$ and $\varepsilon_{WB} = -1.0k_BT_{ref}$. This set of parameters is chosen so that there is a strong attractive interaction between the confining wall and the long-blocks (*B*-blocks) of the copolymers. In this case, it is found that regular structures can be formed for arbitrary pore-length (L_z) at fixed pore diameters D. The morphologies exhibit a weak dependence on the pore length L_z used in the simulation. Furthermore, the simulation results show that, when L_z/L_0 is close to an integer, the final morphology is independent of L_z. Typical morphologies obtained under this optimum condition ($L_z = 40$ lattice spacings or $L_z/L_0 \approx 4$) are plotted in Figure 2a.

Figure 2a shows that as the pore diameter (D) increases, a string of spheres, a single cylinder, a straight band, a twisted band or stacked disks, one-ring structures, a string of spheres at the center and an out one-ring structures, one cylinder and an out one-ring structures, and two-ring structures are observed. The ring structures include helices and stacked toroids. The helices can be single-helices (S-helices) or double helices (D-helices). This sequence of morphological transitions is consistent with the experimental observations and SCFT simulations of Wu et al.[32] This sequence of morphological transitions is also confirmed with the SCFT calculations based on a Gaussian model of diblock copolymers confined in cylindrical pores. [30]

It is interesting to notice that the structures shown in Figure 2a exhibit periodicity along the pore. The nearest-neighbor distance between the cylinders in the helices and the stacked toroids or between the stacked disks have the same value as the equilibrium spacing between the cylinders in the bulk phase. It is more interesting to notice that the structures shown in Figure 2a exhibit a repeating pattern in the radial direction. For larger pores ($D/L_0 > 2.7$), the outer ring of the A-domain forms helices or stacked toroids, whereas the inner A structure evolves from a chain of spheres to a straight cylinder to stacked short cylinders and to stacked toroids or helices. This transition sequence resembles that of the spheres, cylinder, stacked disks, and stacked toroids or helices at smaller pore diameters. A simple calculation for the ringlike morphologies leads to the repeating spacing of about $2L_0$. Therefore, when the pore diameter is increased from D to $D + 2L_0$, one-ring (or four A−B layers) are added to the structure. In another word, one A−B monolayer corresponds to a radial thickness of about $L_0/2$, assuming that the chain conformation is similar to that in the bulk. All these observations indicate that the formation of these novel structures is a consequence of relieving the imposed structural frustrations.

In order to test the robustness of the observed structures, at least six different random number generator seeds have been used to obtain statistically independent results for each pore diameter shown in Figure 2a. Good reproducibility of the morphologies is obtained. Furthermore, the simulations also show that, when simulated with L_z equals to 20, 30, or 50 lattice spacings, the morphological transition sequence is very similar to that showed in Figure 2a. The number of periods of the ring structures along the pore depends on the pore length. When $L_z/L_0 \approx n$ is used in the simulations, the number of the ring structures (the S-helices, the stacked disks and the toroids) is n, whereas the number of the D-helices is $n/2$.

When L_z/L_0 is not an integer, the final morphology does have a weak dependence on the pore length L_z. Examples of this L_z-dependence are shown in Figure 2, parts b and c, for $L_z = 38$ and 42 lattice spacings, respectively. One obvious difference between these results and the ones shown in Figure 2a is that the S-helices region is enlarged when $L_z = 38$ (Figure 2b), whereas the D-helices region is enlarged when $L_z = 42$ (Figure 2c). We have performed a large number of simulations with different pore lengths, and the results indicate that this behavior is generic. That is, when simulated with a fixed cylindrical pore length L_z which is slightly larger than nL_0 (i.e., $nL_0 < L_z < (n + 1/2)L_0$), the region of D-helices is enlarged and the number of D-helices is the same as that obtained with $L_z = nL_0$. When simulated with a fixed cylindrical pore length L_z which is slightly smaller than $(n + 1)L_0$ (i.e., $(n + 1/2)L_0 < L_z < (n + 1)L_0$), the region of S-helices is enlarged and that the number of S-helices (or stacked disks or toroids) is $n + 1$ instead of n. As an example of this generic behavior, typical morphologies and number of periods as a function of L_z are given in Table 1 for a fixed pore diameter $D/L_0 \approx 2.1$. This behavior is also observed for larger cylindrical pore diameters. At $D/L_0 = 2.7-3.3$, D-helices or even triple helices (T-helices) occur in the outer rings when $L_z = 42-44$, and only S-helices or stacked toroids occur when $L_z = 36-38$. At $D/L_0 = 3.9-4.3$, D-helices occur in the inner or outer rings of the coaxial double-ring helices when $L_z = 42-44$, and S-helices or stacked toroids occur in both inner and outer rings when $L_z = 36-38$. Therefore, as suggested by Wang,[20] it is crucial to have a good estimate of L_0 in confined simulations.

Table 1. Typical Example of Morphologies and the Number of Periods As Functions of the L_z Values in the Case Where the Wall Attracts the Majority Blocks with $D/L_0 \approx 2.1$

L_z	morphology	no. of periods
26−30, 36−40, 46−50, 56−60	S-helix	3, 4, 5, 6
20−25, 30−35, 40−45, 50−55, 60−65	D-helix	1, 3/2, 2, 5/2, 3
26−30, 36−40, 46−50, 56−60	stacked toroids	3, 4, 5, 6

Two degenerate structures, the stacked toroids and S-helices, occur simultaneously in Figure 2a−c. This observation indicates that these two closely related morphologies must have similar energies. It is also noticed that three degenerate structures (S-helices, stacked toroids and D-helices) occur at several D/L_0 values in Figure 2a. An analysis of the probability of these three degenerate structures has been carried out by performing a large number of simulations with different random number generator seeds. For a fixed pore diameter $D/L_0 \approx 2.1$, 30 statistically independent simulations have been carried out with $L_z = 40$, resulting in 12 S-helices, 12 D-helices, and 6 stacked toroids. Thus we can conclude that helical structures are the most probable ones. Furthermore, we found that the probability for the formation of the stacked toroids increased with decreasing the number of MCS at each annealing step.

Another important property of the helices is their chirality. Because the block copolymers are achiral, we expect the same number of left-handed and right-handed helices. In the region $D/L_0 = 1.9-2.5$, a large number of independent simulations with different L_z values and different random number generator seeds. 85 S-helices and 55 D-helices were obtained in these simulations. We analyzed the chirality of these helices and found that the ratio of left-handed is 53.0% for S-helices, 62.0% for D-helices. These ratios are consistent with an equal number of left- and right-handed helices. The small deviation from 50% is likely a statistical error due to the small number of simulation samples.

Case 2: $f_A = 1/6$, $\varepsilon_{WA} = -1.0k_BT_{ref}$, and $\varepsilon_{WB} = 1.0k_BT_{ref}$. This set of parameters is chosen so that it leads to a strong attractive interaction between the confining wall and the short blocks (A-blocks) of the copolymers. Essentially the same morphological transition sequence as in case 1 is observed in this case. The observed sequence of morphological transitions is also consistent with the SCFT simulations on a model system of a diblock copolymer melt under the similar confinement. [30] For a fixed pore diameter D, the influence of pore-length L_z on the final morphologies has the same trend as that observed in case 1. For a comparison with case 1, final morphologies with

Table 2. Typical Examples of Morphologies and the Number of Periods As Functions of L_z and D/L_0 in the Case of a Neutral Wall

D/L_0	L_z	morphology	no. of periods
1.4	11−12, 22−24, 32−33	S-helix	1, 2, 3
	13−15, 26−28, 37−41, 48−54	D-helix	$^1/_2$, 1, $^3/_2$, 2
	others (<50)	three cylinders parallel to the cylindrical pore	
1.6	24−28, 35−37, 52, 60	S-helix	2, 3, 4, 5
	15−16, 30−34, 38−41, 50	D-helix	$^1/_2$, 1, $^3/_2$, 2
	46−48, 54	stacked toroids	4, 5
	others (<60)	helices or stacked toroids with defects	
2.9	22−25, 32−33	two-ring S-helices	2, 3
	24−26, 34−40, 46−52	two-ring D-helices helices or stacked toroids with defects	1, $^3/_2$, 2
	others (<50)		

a fixed $L_z = 40$ lattice spacings (L_z/L_0 is close to 4) are plotted in Figure 2d. It has been mentioned that for larger enough pores with the A-blocks form a layer at the wall, increasing the pore diameter (D) further leads to a morphological transition sequence which resembles the transitions observed in case 1 for B-attractive walls.[33] The difference is that the corresponding transitions occur at larger values of D/L_0. This observation can be understood from the fact that, once an A−B monolayer has formed at the pore wall, the system is equivalent to a smaller cylindrical pore with a B-attractive wall. A comparison of the morphologies in Figure 2a and in Figure 2d reveals that the effective diameter of the pore in case 2 is roughly $D - 1.4L_0$. However, the diameter of the equivalent B-attractive pore should be $D - L_0$ if the chain conformation is similar to that of the bulk one. This difference between the observed and ideal values indicates that the chain conformation of polymers close to the walls is different from that in the bulk. The chains near the wall must be stretched strongly in the radial direction. The chain conformation will be analyzed later. After the A-blocks form a layer at the wall and when an effective diameter of the pore is considered, the morphologies in Figure 2d are almost the same as that in Figure 2a. The only difference is that there is a D-helices stable region at $D/L_0 \approx 2.3$ in Figure 2a, which is replaced by two degenerate structures (stacked toroids and S-helices) in Figure 2d.

Case 3: $f_A = {}^1/_6$ and $\varepsilon_{WA} = \varepsilon_{WB} = 0.0k_BT_{ref}$. This set of parameters presents the case of neutral or weakly selective confining walls. For this case, it is found that the morphology strongly depends on the pore-length L_z used in the simulations. For a fixed pore diameter D, regular helical or toroid structures can be formed when L_z is close to a multiple of some special length. Simulations with different pore-lengths L_z were performed so that typical morphologies can be obtained for fixed pore diameter D. Typical examples of the morphologies and the number of periods as functions of L_z and pore diameter are summarized in Table 2. It is apparent that multiple ordered structures can be formed for a given D when different L_z values are used. Those morphologies that can be formed with multi L_z values and have multi periods are chosen as the final equilibrium structures. Structures with four or five periods are summarized in Figure 2e. From Figure 2e, it is observed that there is a preferred segregation of the short blocks to the surfaces although the neutral pore pores have no energetic preference to the blocks. This preferred segregation must be due to an entropic effect. The general trend of the morphological transition is similar to the cases of selective walls (case 1 and 2). However, there are noticeable differences. One difference is that straight cylinders oriented both parallel or nearly perpendicular to the cylindrical pore are found. The former are observed in a very narrow range of $D/L_0 \approx 1.2$ (three A-cylinders) and $D/L_0 \approx 2.0 \pm 0.2$ (one cylinder at the pore center and four, five, and six A-cylinders at the pore wall, denoted as C_{14}, C_{15}, and C_{16}, respectively). These morphologies are similar to the two-dimensional structures obtained by Li, Wickham, and Garbary.[29] The perpendicular cylinders are observed at $D/L_0 \approx 2.5$ and 3.5. Besides these straight cylindrical structures, other structures, such as one cylinder at the pore center and quadruple helices (Q- helices) (denoted as C_1H_4) or T-helices (denoted as C_1H_3) at the pore wall occurs at $D/L_0 \approx 1.8-2.0$ or 2.2, are also observed. However, the period of the Q-helices is very long. One-ring, one cylinder at the pore center and out one-ring, two-ring, and one-cylinder at the pore center and two-ring helical structures are formed at $D/L_0 \approx 1.5$, 2.2, 3.0, and 3.7, respectively. We notice that the regions for one-ring or two-ring of D-helices are relatively larger, and the degenerated structures of stacked toroid and S-helices also occur just before the transitions from one-ring helices to one cylinder at the center with an outer ring of cylinders or helices. For the small A-droplets and cylinders both oriented parallel or nearly perpendicular to the cylindrical pore, the characteristic period of the final morphologies are the same as the bulk cylinder spacing. Whereas for all the S-helical or toroid structures with both one-ring and one cylinder at the pore center and out one-ring, the characteristic period is about $1.1-1.3L_0$, for all the D-helical structures with both one-ring and two-ring, the characteristic period is about $2.2-2.5L_0$ and for all the T-helical structures the characteristic period is about $3.3L_0$. That is, the characteristic distances of helical or toroid structures are slightly larger than the period in the bulk. We also notice that the radial period for the helical structures is also about $2L_0$, the same as that of selective wall.

Figure 2e shows that more complex structures are formed in this special case due to the extra frustration provided by the neutral wall. Although exact neutral wall is not likely to occur in experimental systems, one expects that similar behavior as the neutral wall case should be observed for weakly selective walls for the short blocks. Therefore the predictions for this case can be used to compare with some experimental observations. Our prediction that one layer of helices forms when $D/L_0 = 1.1-1.6$ is in good agreement with the experimental observations of Xiang and co-workers on cylinder-forming asymmetric PS-*b*-PBD diblock copolymers confined within cylindrical nanopores in an alumina membrane.[28] In their experiments, one ring of multiple helices is observed for the cylinder-forming diblock copolymer within the nanopores with diameters D of 33−45 nm ($D/L_0 = 1.1-1.5$).

Property of the Helices. A variety of confinement-induced structures have been observed, as shown in the last section. Among these interesting morphologies, helices present a common structure as shown in Figure 2. It turns out that the formation of helices in the diblock copolymer system studied in this paper can be understood based on a packing mechanism. The basic assumption is that, because the system is in strong segregation region, the block copolymers have a strong preference to keep their self-assembled cylindrical shape with a fixed diameter d. Formation of cylinders with a diameter larger or smaller than the equilibrium diameter, or distortions of the cylinders, will lead to a high energy cost. For a cylindrical pore with a diameter D and a length L_z, the length of the self-assembled cylinder with a fixed diameter d is easily obtained,

$$L = f_A\left(\frac{D}{d}\right)^2 L_z \tag{1}$$

For very small pore diameters, the length of the self-assembled cylinder will be much shorter than the pore length, $L \ll L_z$. Formation of a straight cylinder with a length equals to the L_z will lead to a thin cylinder with a diameter less than d. Because the formation of a thinner cylinder at the center of the pore will lead to a high energy cost, the formation of a cylinder is prohibited. Instead the copolymers assemble into a string of spheres. Assuming that the self-assembled cylinders have the same diameter as the cylinders in the bulk $d/L_0 = [2(3^{1/2})f_A/\pi]^{1/2}$, we have $L/L_z = [\pi/(2(3^{1/2})](D/L_0)^2$. Therefore the condition $L < L_z$ leads to $D/L_0 < 1.05$, which is consistent with the condition for the formation of a string of spheres ($D/L_0 < 0.7$).

For larger pore diameters, the length of the self-assembled cylinder is longer than the pore length, and packing of such a long stringlike subject into a short space naturally leads to the formation of helices. Assuming that this mechanism is correct, we can calculate the radius and pitch of these helical structures as follows. Figure 3 shows the basic schematics of a single helix, in which S is the period or the linear length of one turn of the S-helix, R is the radius of the S-helix. If a single turn of the S-helix is stretched flat, one obtains the right triangle shown on the right side of Figure 3, where $C = 2\pi R$ is the circumference of the turn and L' indicates the length of the string required to obtain a full turn. From these definition we have $L' = [(2\pi R)^2 + S^2]^{1/2}$. On the other hand, the length of the self-assembled cylinder is given by 1 with $L_Z = S$. Equating these two lengths immediately leads to a relationship between the radius of the S-helix and the diameter of the pore,

$$R_S = \frac{S}{2\pi}\sqrt{f_A^2\left(\frac{D}{d}\right)^4 - 1} = \frac{S}{2\pi}\sqrt{\frac{\pi^2}{12}\left(\frac{D}{L_0}\right)^4 - 1} \tag{2}$$

The pitch of the S-helix can be described by the tilted angle α_S, which can be easily obtained from the geometric relations shown in Figure 3,[30,41]

$$\sin\alpha_S = \frac{S}{L'} = \frac{L_z}{L} = \frac{d^2}{f_A D^2} = \frac{2\sqrt{3}}{\pi}\left(\frac{L_0}{D}\right)^2 \tag{3}$$

Similar relationships can be derived for the double helices,

$$R_D = \frac{S_D}{2\pi}\sqrt{\frac{\pi^2}{48}\left(\frac{D}{L_0}\right)^4 - 1} \tag{4}$$

$$\sin\alpha_D = \frac{4\sqrt{3}}{\pi}\left(\frac{L_0}{D}\right)^2 \tag{5}$$

These simple relations show that the simple model predicts the tilted angle (α), helix radius (R), and cylinder length (L/L_z) are functions of the ratio D/L_0. The general trend is that L/L_z and R are increasing functions of D/L_0, while the pitch angle α is a decreasing function of D/L_0. At the limit $D/L_0 \gg 1$, the tilted angle of the double helices is twice of that for the single helices.

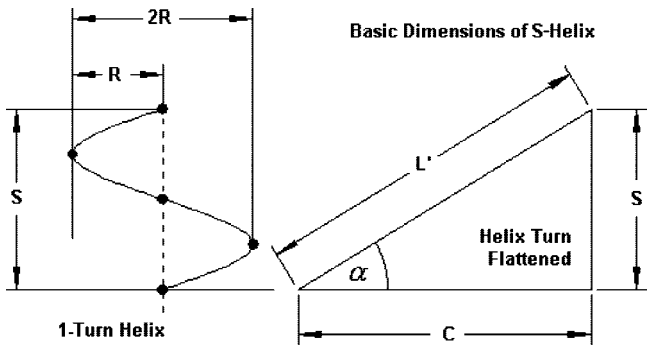

Figure 3. Basic dimensions of a helix.

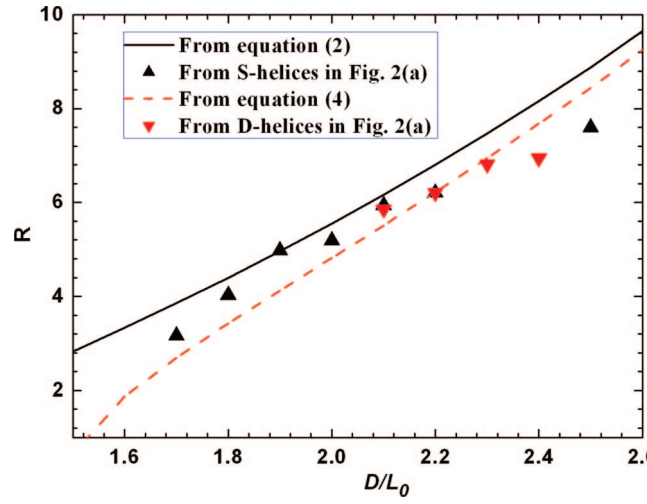

Figure 4. Radius R of a helix as a function of the ratio D/L_0 for both S-helix and D-helix.

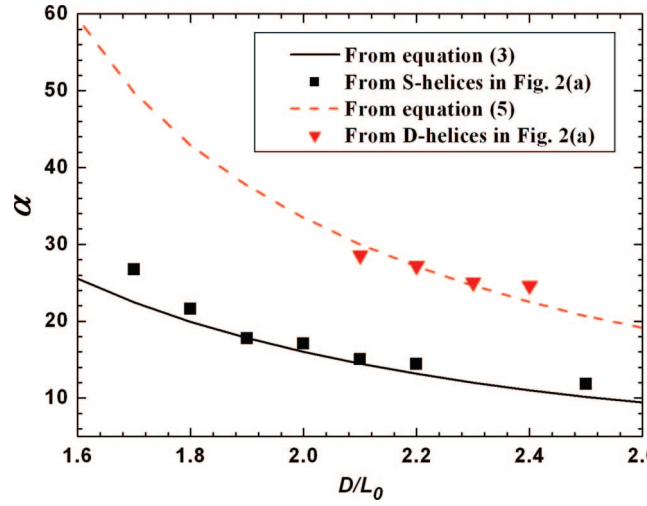

Figure 5. Pitch angle α of a helix as a function of the ratio D/L_0 for both S-helix and D-helix.

In order to test these relationships, the helices obtained from simulations are analyzed and the properties of the helices are computed. The results are presented in Figures 4, 5, and 6, where the helix radius R, pitch α, and cylinder length (L/L_z) of both S-helices and D-helices are plotted as functions of the ratio D/L_0 for the case where the wall attracts the majority blocks (case 1 from Figure 2a). The corresponding analytic predictions (1–5) are also plotted in these figures. The agreement between the computed values and the model predictions is surprisingly good, considering that there are no adjustable parameters. This agreement indicates that the proposed mechanism of helix formation is a reasonable description of our simulated system. It is also noticed that the computed values (symbols) in the large or smaller D/L_0 regions deviate from their theoretical lines (Figures 4 and 6). The deviations in Figure 4 and 6 indicate that the radius (R) and cylinder length (L/L_z) of the helices in Figure 2a are smaller than that of the corresponding ideal helices. This implies that the assumption of self-assembled cylinders with a fixed diameter must be violated in these cases. Indeed deformations of the self-assembled cylinders occur in these regions. For large D/L_0

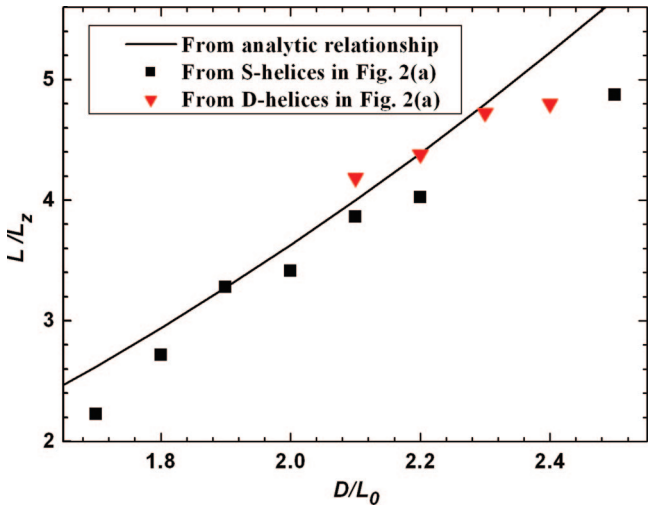

Figure 6. Helix length (L/L_z) as a function of the ratio D/L_0.

=2.4−2.5, it is observed that the cylinders are with a larger diameter, whereas for small $D/L_0 \approx 1.7$, the S-helices are made of a flattened cylinder.

From the results shown in Figure 4, it can be noticed that for a given value of D/L_0, the radius (R) of an S-helix is slightly larger than that of a D-helix. Further simulation results also demonstrate (not shown) that, for the degenerate structures (S-helices, stacked toroids and D-helices) at $D/L_0 = 2.1-2.2$, the radius R of the ring structure and the radius of the cylinder that forms the structure are increasing in the order of stacked toroids > S-helices> D-helices. Another observation is that the radius (R) of the helical structures satisfies $0.6L_0 < 2R < 1.6L_0$ for the S-helices and $1.1L_0 < 2R < 1.4L_0$ for the D-helices. Theoretically the radius can be any positive nonzero value, if the self-assembled cylinders can be deformed. In practice, R should satisfy $2R > d$ to form helices made of a cylinder with a diameter of the bulk phase (d). This condition is satisfied for the helices shown in Figure 4. It is also noticed that the D-helices can be formed only when $2R > L_0$.

The pitch angle α_D (Figure 5) of a D-helix is larger than $2\alpha_S$ for smaller D/L_0, where α_S is the pitch angle of an S-helix. For larger pore diameter the ratio of these two pitch angles approaches 2. Specifically, α_S is in the range of 10 to 30° when one-ring of S-helices are formed, and α_D is in the range of 20 to 30° when one-ring of D-helices are formed. Li and Wickham also computed the pitch angles of S-helix and D-helices for the simulated helices and compared them with those deduced at the SSL, where good agreement was obtained between the two results.[30]

Figure 6 shows that the cylinder length (L/L_z) is in the range of 2−5 when one-ring of S-helices are formed, and it is in the range of 4−5 when one-ring of D-helices are formed. Combining the results of Figure 4 and Figure 6, it can be concluded that the distance between the cylinders is less than L_0 if straight cylinders with a diameter similar to that in the bulk are formed inside the pores. In another word, two such straight cylinders inside the pores will lead to large compression energy. The helices are structures which minimize the total energy.

For case 2, in which the wall attracts the minority blocks, the pitch angle α_S of the S-helices as a function of the ratio D/L_0 is plotted in Figure 7. In this figure the symbols are calculated from the one-ring S-helices after the A-blocks form a layer at the wall, as shown in Figure 2d. It is noticed that the morphology in Figure 2d with a pore diameter parameter of D/L_0 is similar to the morphology in Figure 2a with a smaller effective pore diameter of D/L_0 −1.4. The corresponding analytic prediction ($\sin \alpha_S = [(2(3^{1/2}))/\pi]/[1/(D/L_0 - 1.4)^2]$) is

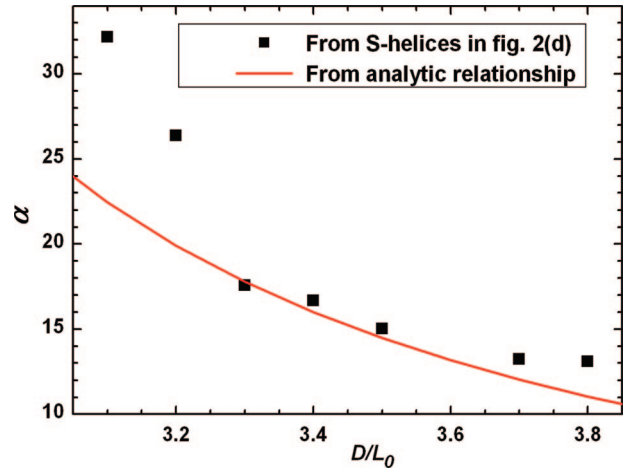

Figure 7. Pitch α of a helix as a function of the ratio D/L_0 for the one-ring helices plotted in Figure 2d after the A-blocks form a layer at the wall.

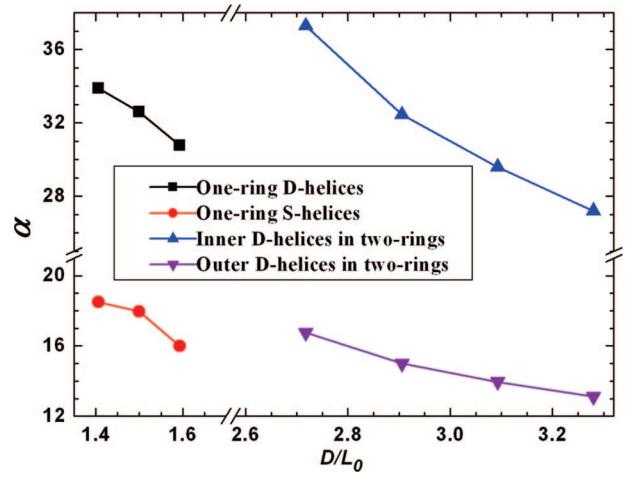

Figure 8. Pitch angle α of helices as a function of the ratio D/L_0 for the one-ring and two-ring helices plotted in Figure 2e.

also plotted in Figure 7. The agreement between the computed values and the model predictions is good for $3.3 < D/L_0 < 3.6$. The larger angles of the first two data points are due to the larger period of the S-helices formed at $D/L_0 < 3.3$. The curve in Figure 7 has the same trend as the curve for S-helices in Figure 5, and the α values are in the same range as that for the one-ring S-helices in case 1. Comparing Figure 7 with Figure 5, it is noticed that the α values are very close for the same morphologies in Figure 2d and Figure 2a. Compared with the helical structures shown in Figure 2a or Figure 2d, the one-ring helices or the out-ring helices of the two-ring structures shown in Figure 2e are made of a distorted or flattened cylinder. The origin of the distorted cylinder is due to the fact that the helices are in the proximity of the pore wall. Our results show that for the same amount of the A-blocks, the unit length of a helix formed with the flattened cylinder is longer than that of a helix formed with a cylinder that has the bulk diameter. The D/L_0 values are smaller for the occurrences of the one-ring or two-ring helical structures in the case of neutral wall than in the case of a B-attractive wall. For the one-ring or two-ring helical structures shown in Figure 2e, the pitches as a function of the ratio of D/L_0 are plotted in Figure 8. It can be seen that, for the one-ring S-helices the α values are in the range of 16 to 19°, in good agreement with these observed experimentally.[28] For the one-ring D-helices, the α values are in the range of 30 to 34°, which is almost two times that for the S-helices. For the two-ring helical structures shown in Figure 2e, the α values

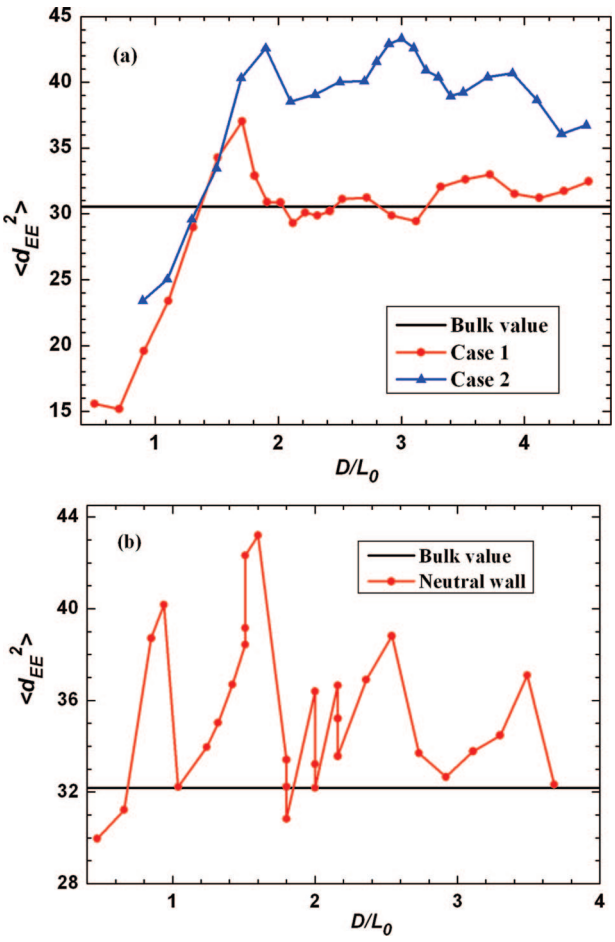

Figure 9. Mean square end-to-end distance of chains $\langle d_{EE}^2 \rangle$ as a function of the ratio D/L_0 for different wall-polymer interactions. (a) The cases where the wall attracts the majority blocks (case 1) and the minority blocks (case 2). (b) The case of a neutral wall (case 3).

are in the range of 26 to 37°. For those inner-ring D-helices when $2.7 < D/L_0 < 3.3$, the α values have similar trend as the curve for the D-helices shown in Figure 5 when $1.7 < D/L_0 < 2.3$, i.e., one period smaller. For the outer-ring D-helices of the two-ring helical structures shown in Figure 2e, the α values are in the range of 13 to 17°.

Mean-Square End-to-End Distance. In order to gain insights into the confinement effects on the chain conformations, the mean-square end-to-end distance of the chains (denoted by $\langle d_{EE}^2 \rangle$) is computed, and plotted in Figure 9 as a function of D/L_0. As a comparison, the bulk values of $\langle d_{EE}^2 \rangle$ is also plotted in Figure 9. From the computations it is noticed that the degenerate structures in Figure 2 have very similar values of $\langle d_{EE}^2 \rangle$. The average value of $\langle d_{EE}^2 \rangle$ for the degenerate structures is plotted in Figure 9. There are, however, exceptions. For some degenerate structures such as these shown in Figure 2e, different $\langle d_{EE}^2 \rangle$ values are obtained (Figure 9b). The mean square end-to-end distance $\langle d_{EE}^2 \rangle$ as a function of D/L_0 for case 1 and case 2 is plotted in Figure 9a. The first fact to notice is that the bulk value of $\langle d_{EE}^2 \rangle^{1/2}$ is slightly larger than $L_0/2$, implying that the blocks are in a stretched state. Furthermore, the end-to-end distance of the chains under confinement varies with D/L_0 and with the polymer-wall interactions. Let us consider the case with a strong wall-majority attractive interaction (case 1) first. For small pores with $D/L_0 < 1.0$, the mean square end-to-end distance is much smaller than the bulk value, indicating that the chains are strongly compressed due to the tight confinement. For larger pores with $D/L_0 > 1.0$, the mean square end-to-end distance oscillates as a fuction of D/L_0 about the bulk value. The minima of $\langle d_{EE}^2 \rangle$v occur when D/L_0 is close to an integer and the maxima occur when D/L_0 is roughly a half-integer. This oscillative behavior of $\langle d_{EE}^2 \rangle$ indicates that the chain conformation is close to that in the bulk at integer D/L_0, and that the chains are slightly stretched at half-integer D/L_0. It is also noticed that, as D/L_0 is increased, the amplitude of the oscillation decreases and $\langle d_{EE}^2 \rangle$ approaches the bulk vlaue. This observation indicates that the confinement effect weakens with the increase of the pore size. Very similar oscillative behavior of $\langle d_{EE}^2 \rangle$ with D/L_0 has been observed in symmetric diblock copolymers confined in cylindrical pores with strongly selective surfaces[21] and also in symmetric diblock copolymers confined between two parallel and strongly selective surfaces.[39] Comparing Figure 2a and Figure 9a, it is interesting to notice that the peak values of $\langle d_{EE}^2 \rangle$ correspond to the morphologies just before the transitions from the one-cylinder to the one-ring structures, or from the one-ring to a chain of spheres at the center and an outer one-ring structures, or from the one cylinder at the center and an outer one-ring to two-ring structures. Therefore, we can conclude that the morphological transitions are driven by the release of structural frustrations in the form of stretching energy.

We now turn our attention to the case with a strong wall-minority attractive interaction (case 2). As shown in Figure 9a, the mean square end-to-end distance $\langle d_{EE}^2 \rangle$ in this case also oscillates as a fuction of D/L_0. However, in this case $\langle d_{EE}^2 \rangle$ oscillates about a value which is much higher than the bulk value of $\langle d_{EE}^2 \rangle$. This larger baseline value of $\langle d_{EE}^2 \rangle$ originates from the fact that, with a strong wall−minority attractive interaction, the minority blocks (A-blocks) are forces to the wall. Therefore the short blocks occupy the outer region of the cylinder while the long blocks are inside it, forming a reversed cylinder. This morphological difference naturally leads to a large baseline $\langle d_{EE}^2 \rangle$ because the outermost short blocks have to be strongly stretched. The polymer chains in case 2 are strongly stretched when the *A*-blocks form a layer at the wall, and $\langle d_{EE}^2 \rangle$ reaches its first maxmum when a chain of spheres is formed at the center. Comparing Figure 9a with parts a and d of Figure 2, it is noticed that the maxima and minima of $\langle d_{EE}^2 \rangle$ curves in Figure 9a correspond to the same morphologies in parts a and d of Figure 2, respectively. Therefore, we can conclude that when an effective B-attractive wall cylindrical pore of diameter $D_{eff} = D - 1.4L_0$ is considered in case 2, the mean square end-to-end distance assumes minima when D_{eff}/L_0 is close to an integer and maxima when D_{eff}/L_0 is close to a half-integer.

For the special case of neutral walls (case 3), Figure 9b shows that the mean square end-to-end distance oscillates as a fuction of D/L_0. Furthermore, $\langle d_{EE}^2 \rangle$ also exhibits minima at integer D/L_0 and maxima at half-integer D/L_0. These features are similar to that in case 1 and case 2. Comparing Figure 2e and Figure 9b, we notice that the maxima of $\langle d_{EE}^2 \rangle$ also correspond to the morphologies just prior to the transitions between different morphologies. We also notice that the minma of $\langle d_{EE}^2 \rangle$ are very close to the bulk value of $\langle d_{EE}^2 \rangle$ and that the average value of $\langle d_{EE}^2 \rangle$ is higher than the bulk value. The reason for the higher average value of $\langle d_{EE}^2 \rangle$ in this case is that the minority blocks tend to segregate to the walls due to an entropic effect. On the other hand, the entropic effect is not a very strong effect, thus the neutral case is different from case 2. In the neutral-wall case, the majority blocks can occupy sites both the outer region of the cylinder and the inside with smaller circles of the cylindrical pores since the minority blocks cannot occupy all sites in the outer region with bigger circles. Thus a longer period in the *z*-direction means a larger proportion of the majority blocks is in the bigger circle, which is the reason that the period in the *z*-direction is larger in this neutral-wall case than that in the bulk. For the degenerate structures at $D/L_0 \approx 1.5$, the $\langle d_{EE}^2 \rangle$ values are ordered according to D-helices < stacked toroids <

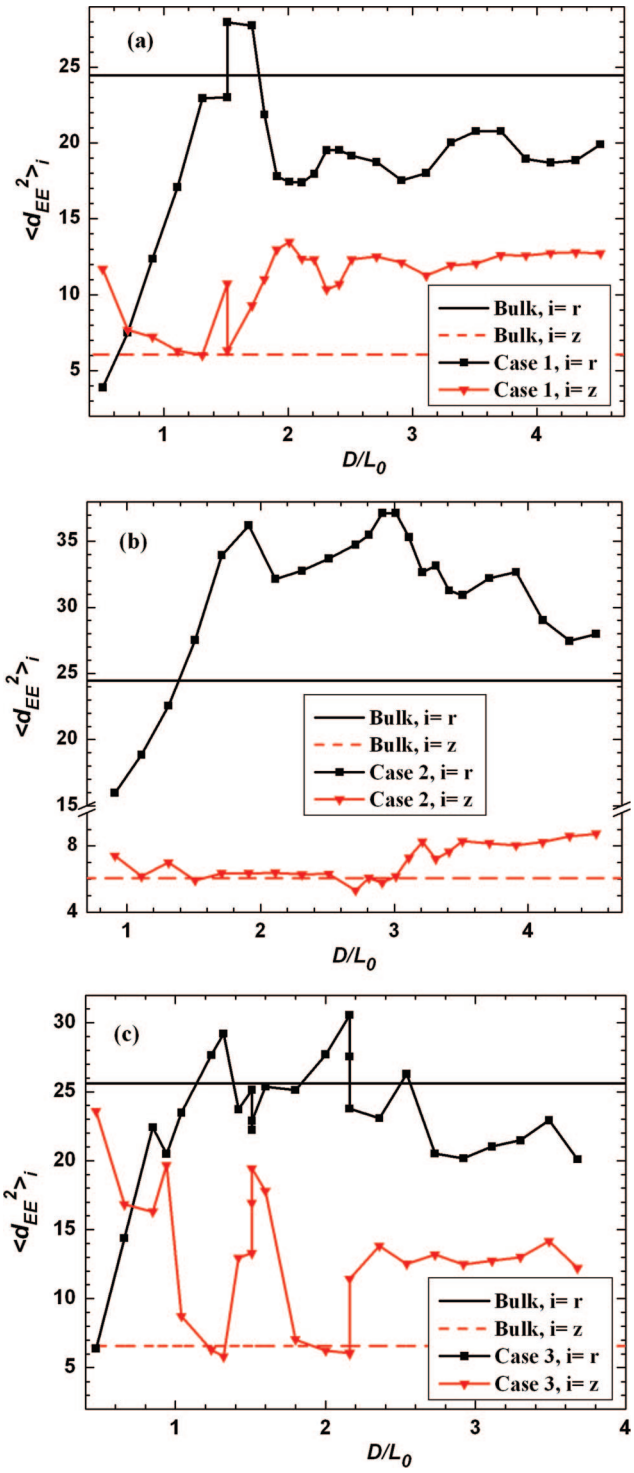

Figure 10. Components of the end-to-end distance along the radial and the axis directions of the cylindrical pore as a function of D/L_0 for the three cases: (a) the case where the wall attracts the majority blocks (case 1); (b) the case where the wall attracts the minority blocks (case 2); (c) the case of a neutral wall (case 3).

S-helices. For the degenerate structures at $D/L_0 \approx 1.8-2.2$, the $\langle d_{EE}^2 \rangle$ values are ordered according to $C_{15} < C_{14} < C_1H_4$ and $C_{15} < C_1H_4 < C_{14}$ and $C_{16} < C_1H_3 < C_{15}$, respectively.

In order to gain a better understanding of the chain conformations under confinement, the components of the mean square end-to-end distance, $\langle d_{EE}^2 \rangle_r = \langle d_{EE}^2 \rangle_X + \langle d_{EE}^2 \rangle_Y$ and $\langle d_{EE}^2 \rangle_Z$, are computed. These quantities are plotted in Figure 10a−c as a function of D/L_0 for the three cases, respectively. As a comparison, the corresponding components of $\langle d_{EE}^2 \rangle$ for the hexagonally packed cylinders in the bulk are also plotted in Figure 10. For some of the degenerate structures shown in Figure 2, different values of the components of $\langle d_{EE}^2 \rangle$ are obtained, which are plotted in Figure 10 as well. It is interesting to notice that, for the two block copolymers used in the simulations, the two components of the end-to-end distance in the bulk are very different, $\langle d_{EE}^2 \rangle_Z$ is far less than $\langle d_{EE}^2 \rangle_r$. Therefore the chains in the hexagonally packed cylinders in the bulk are mainly stretched in the radial directions.

Figure 10a shows the components of $\langle d_{EE}^2 \rangle$ for the case where the wall is strongly attractive to the majority blocks (case 1). It shows that for small pores, in which a chain of spheres is formed, the *r*-component of $\langle d_{EE}^2 \rangle$ is strongly compressed while the *z*-component is stretched, as compared with their corresponding bulk values. When the pore size increases to the region where a single straight cylinder is formed, $\langle d_{EE}^2 \rangle_r$ is increasing while $\langle d_{EE}^2 \rangle_Z$ is decreasing with the increase of D/L_0. At the pore size just before the transition from a single straight cylinder to a stack of tilted disks ($D/L_0 \approx 1.3$), $\langle d_{EE}^2 \rangle_r$ and $\langle d_{EE}^2 \rangle_Z$ are all very close to their corresponding bulk values, implying that the self-assembled cylinders are similar to the bulk ones in this region. $\langle d_{EE}^2 \rangle_r$ for the stacked tilted disks at $D/L_0 \approx 1.5$ is similar to that for the cylinders at $D/L_0 \approx 1.3$, whereas $\langle d_{EE}^2 \rangle_Z$ is much larger than that for the latter. $\langle d_{EE}^2 \rangle_r$ arrives at its maximum value when a twisted band structure is formed at $D/L_0 \approx 1.5$ whereas $\langle d_{EE}^2 \rangle_Z$ is similar to that of the bulk value. For larger pores where helical or a stack of toroid structures are formed, compared with their corresponding bulk values, the *z*-component of the end-to-end distance is strongly stretched, while the *r*-component is heavily compressed. For the degenerate structures (S-helices, stacked toroids, and D-helices) at $D/L_0 \approx 2.1-2.2$, the $\langle d_{EE}^2 \rangle_r$ values are ordered according to stacked toroids < S-helices< D-helices, whereas the $\langle d_{EE}^2 \rangle_Z$ values are in the reversed order. The maximum difference of $\langle d_{EE}^2 \rangle_r$ or $\langle d_{EE}^2 \rangle_Z$ between two adjacent structures is less than 2. It is interesting to find that for the D-helices at $D/L_0 \approx 2.1-2.4$, $\langle d_{EE}^2 \rangle_r$ is increasing slowly with the increase of D/L_0 (from 18.52 to 19.54), whereas $\langle d_{EE}^2 \rangle_Z$ stays roughly a constant (it range is 10.34∼10.92). Therefore in these D-helices $\langle d_{EE}^2 \rangle_r \approx 2\langle d_{EE}^2 \rangle_Z$, or $\langle d_{EE}^2 \rangle_X \approx \langle d_{EE}^2 \rangle_Y \approx \langle d_{EE}^2 \rangle_Z$. For the degenerate structures at $D/L_0 \approx 2.7$ or larger, the components of $\langle d_{EE}^2 \rangle$ approach certain constant values which are not obviously related to the bulk values.

Figure 10b shows the components of $\langle d_{EE}^2 \rangle$ for case 2. The obvious characteristic is that for larger pores where the *A*-blocks have formed a layer at the wall, the *r*-component of $\langle d_{EE}^2 \rangle$ is strongly stretched when compared with its corresponding bulk value. As mentioned above, in this case the minority blocks of the copolymer chains occupy the sites in the bigger circle, and the majority blocks occupy the sites in the smaller circle. Our results show that the majority blocks are strongly stretched in the radial direction in this case, leading to a much higher $\langle d_{EE}^2 \rangle_r$ than the bulk value. Figure 10b shows that with the small pores where the A-blocks cannot form a layer at the wall, the radial component of the end-to-end distance is increasing with the increase of D/L_0, the *z*-component of $\langle d_{EE}^2 \rangle$ is kept to a value that is close to the corresponding bulk value. For larger pores after the *A*-blocks formed a layer at the wall, the variation trend of the two components with the increase of D/L_0 is very similar to that shown in Figure 10a but at a smaller pore diameter. However, the curve of the *r*-component is higher and the curve of the *z*-component is lower in Figure 10b than the corresponding curves in Figure 10a due to the existence of one A-layer at the wall. The larger *r*-component value for chains near to the wall resulted in a smaller average variation range in curves in Figure 10b than that in curves in Figure 10a.

Figure 10c shows the components of $\langle d_{EE}^2 \rangle$ for the case of neutral wall (case 3). Its obvious characteristic is that the z-component is strongly stretched except at those points where cylinders parallel to the pore are formed. As analyzed above, the chain-stretching in the z-direction can increase the proportion of the majority blocks in the bigger circle. For small pores, when a chain of spheres is formed, the r-component of $\langle d_{EE}^2 \rangle$ is strongly compressed compared with its bulk value. When the pore size is increased to where cylinders parallel to the cylindrical pore are formed, the r-component is slightly stretched compared with its corresponding bulk value, whereas the z-component is very close to its corresponding bulk value. This is because that when cylinders parallel to the pore are formed, the proportion of the majority blocks in the bigger circle does not change through increase the period in the z-direction, and thus it is similar to that of case 2 and resulted in the chain stretching in the r-direction. Since the minority blocks of the copolymer chains can only occupy parts of sites in the bigger circle, the chain stretching is smaller in this case. At the pore sizes where helical or stacked toroid structures are formed, compared with its bulk value the r-component is compressed, which is consistent with that in the selective walls but the degree of compression is smaller. At the pore sizes where cylinders nearly perpendicular to the pore are formed, our results show that in each cylinder, the component of $\langle d_{EE}^2 \rangle$ along the axis of the cylinders is considerably smaller than the component along the direction perpendicular to the axis of the cylinders, similar to the bulk case. Since the axis of the cylinders is not totally perpendicular to the axis of the pore, the two components are all changed compared with their respective bulk values. For the degenerate structures (S-helices, stacked toroids and D-helices) $D/L_0 \approx 1.5$, the $\langle d_{EE}^2 \rangle_r$ values are ordered according to stacked toroids < S-helices < D-helices, whereas the $\langle d_{EE}^2 \rangle_Z$ values are ordered according to D-helices < stacked toroids < S-helices. The order of the $\langle d_{EE}^2 \rangle_r$ values is consistent with that in the case 1 and case 2, whereas the order of the $\langle d_{EE}^2 \rangle_Z$ values is not totally consistent with that in the selective wall cases. For the degenerate structures at $D/L_0 \approx 1.8-2.2$, the $\langle d_{EE}^2 \rangle_r$ values are ordered according to $C_{15} < C_1H_4 < C_{14}$ and $C_{15} < C_1H_4 < C_{14}$ and $C_1H_3 < C_{16} < C_{15}$, respectively, whereas the $\langle d_{EE}^2 \rangle_Z$ values are ordered according to $C_{14} < C_{15} < C_1H_4$ and $C_{14} < C_{15} < C_1H_4$ and $C_{16} \approx C_{15} < C_1H_3$, respectively. It is interesting to find that for D-helices at $D/L_0 \approx 1.4-1.5$, the chain conformation is roughly isotropic, i.e., $\langle d_{EE}^2 \rangle_r \approx 2 \langle d_{EE}^2 \rangle_Z$.

From the above analysis of the three cases, it can be concluded that the two components of $\langle d_{EE}^2 \rangle$ for the polymer chains depend on the morphologies and have the following general trends. (1) For cylinder morphologies in the bulk or cylinders parallel to the cylindrical pore in the confinement, the z-component of $\langle d_{EE}^2 \rangle$ is considerably smaller than the r-components. (2) When the morphology of a string of spheres is formed at the small pore, the r-components of $\langle d_{EE}^2 \rangle$ are strongly compressed while the z-components are strongly stretched compared with their respective bulk values. (3) For the helical or stacked toroid structures induced by the confinement, compared with their corresponding bulk values the z-component of $\langle d_{EE}^2 \rangle$ is strongly stretched, while the r-component is compressed. (4) For the one-ring D-helices, the chain conformations are roughly isotropic, i.e., $\langle d_{EE}^2 \rangle_X \approx \langle d_{EE}^2 \rangle_Y \approx \langle d_{EE}^2 \rangle_Z$.

Energitics of Different Structures. To shed further light into the complex phase behavior observed in the confined system as a function of D/L_0, the free energy of some selected structures is analyzed. For the confined block copolymers, the free energy contains contributions from three sources: (1) the monomer−surface interactions, (2) the monomer−monomer interactions, and (3) the entropic cost of stretching chains in the segregated morphologies. The equilibrium morphology of the block copolymers under confinement should be the result of the competition between these three contributions. In what follows these contributions are estimated for case 1 at small D/L_0 region in which a string of spheres, a single cylinder, and a single helix are formed. A comparison of the free energies for these three structures confirms that they are indeed structures minimizing the free energy.

Qualitatively, the monomer−surface interactions are related to the local concentration profile of the monomers near the surface (surface energy). This contribution is identical for different morphologies at a given D in case 1. This is due to the fact that the B-monomers form a layer near the pore surfaces for all the morphologies. Therefore we can neglect this component in the comparison of the free energy of different structures. In a phase-separated system, the A−B monomer interactions can be attributed to interfacial energy which is due to the contact between unlike monomer domains. This contribution is proportional to the A−B interfacial area of the morphology. The interfacial area can be estimated based on the fact that the total volume of A-domains is equal to that of all A-monomers. When a string of spheres is formed in the pore, the interfacial area of one sphere can be expressed as

$$S_S = 4\pi\left(\frac{d_S}{2}\right)^2 = \pi\left(\frac{3}{8} f_A D^2 L_z\right)^{2/3} \quad (6)$$

where d_S is the diameter of the spheres. In eq 6, we assume that the spheres are equal in size and their period is L_0. When a cylinder is formed in the pore, the interfacial area can be expressed as

$$S_C = \pi d_C L = \pi\sqrt{f_A} D L_z \quad (7)$$

where d_C is the diameter of the cylinder. When a helix is formed in the pore, we assume that the diameter of cylinder is identical to that of cylinder in the bulk (equal to d), thus its length can be calculated using eq 1. The interfacial area for a helical structure can be expressed as

$$S_H = \pi d L = \pi d f_A \left(\frac{D}{d}\right)^2 L_z \quad (8)$$

For a given structure, the free energy contribution from the A−B monomer interaction can then be estimated as the interfacial area times the interfacial free energy per unit area, or the interfacial tension. In our model, the interfacial tension is specified by the A−B interaction ε_{AB}.

The entropic contribution can be estimated by measuring the mean-square end-to-end distance of the chains, which characterize the chain stretching. In our model system, a diblock copolymer chain can be considered as a sequence of N (=12) freely joined segments of length b; the conformational entropy of such a chain is a maximum if it is completely unconstrained. Constraining its ends to have a separation R leads to a conformational entropy reduction of $\Delta S = -3k_B R^2/2Nb^2$, and a free energy increase of $\Delta F = 3k_B T R^2/2Nb^2$,[21,39] where T is the temperature, b^2 is the square of the average of all the allowed bond length with a value of 1.6285, and $R^2 = \langle d_{EE}^2 \rangle$. Our results shown in Figure 9a indicate that $\langle d_{EE}^2 \rangle$ increases nearly linearly with D/L_0 when a single cylinder is formed in the pore, therefore we assume that $\langle d_{EE}^2 \rangle = \alpha D/L_0$ for the assumed structures of a single cylinder and that of a string of spheres, and the parameter α can be estimated by fitting the curve of case 1 in Figure 9a. Figure 9a also indicates that $\langle d_{EE}^2 \rangle$ is approaching to the bulk value for structures with one-ring of the helix; thus, the bulk value of $\langle d_{EE}^2 \rangle$ is used for the assumed helical structures.

On the basis of these estimates, we can approximate the free energy per diblock copolymer chain for the observed and assumed structures as $F = N\varepsilon_{AB} S_{AB}/V_C + \Delta F$, which correspond

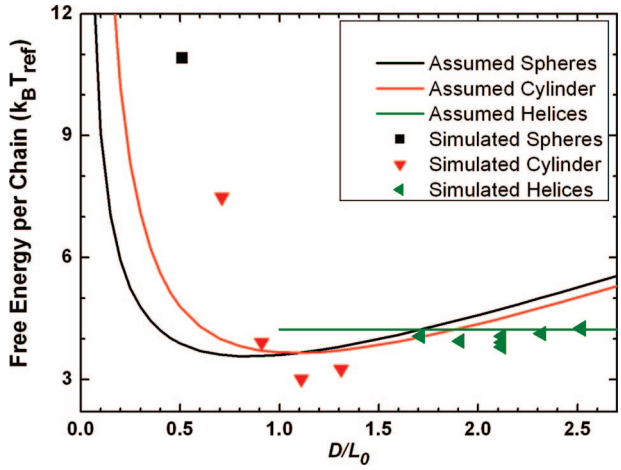

Figure 11. Free energy per chain F as a function of D/L_0.

to the interfacial and stretching contributions. In this expression S_{AB} and V_C are the total A−B interfacial area and the volume of the cylindrical pore, respectively. This free energy is computed in two ways. In the first method the different quantities in the expression are computed from the simulated structures (Figure 2), the results are plotted in Figure 11 as symbols. In the second method, S_{AB} is computed using eqs 6–8 for assumed spheres, cylinder, and helix, respectively, α is computed by fitting the mean square end-to-end distance shown in Figure 9a in the range $D/L_0 \in [0.7, 1.3]$, and the results are plotted as curves in Figure 11. Considering that to form helices consisting of cylinder with a diameter identical to that of cylinder in the bulk, the pore diameter D must be larger than L_0, we plotted the free energy for the assumed helical structures only for $D/L_0 \geq 1.0$. From Figure 11, it is clear that the free energy for the spherical structure is the lowest when D/L_0 is smaller than ~1.0, and that for the helical structure is the lowest when D/L_0 is larger than ~1.9, and between the two values, the free energy for the a straight cylinder is the lowest. This sequence of different structures and the boundaries between them are consistent with the simulation results, indicating that the free energy argument for these structures is reasonable. From Figure 11, we also notice that the values of free energy from the model structures almost coincide with those for the simulated structures when $D/L_0 > 0.9$, whereas the former are much lower than the latter at smaller D/L_0. The reason for the deviation is that the cross-section of the cylinder or the spheres is not exactly circular in the simulated structure due to the lattice model, especially at smaller D/L_0, the deviation from a circular is larger. Therefore the simulated structures possess larger interfacial areas.

Conclusion

Equilibrium morphologies of cylinder-forming asymmetric diblock copolymers confined in cylindrical pores are studied using a simulated annealing method. Three representative cases are considered. It is discovered that the two-dimensional confinement in the form of cylindrical pores leads to a rich variety of novel morphologies. Some of these structures cannot form in unconfined or one-dimensional confined systems. The equilibrium morphology is largely controlled by the ratio between the pore diameter D and the bulk cylinder spacing L_0 (D/L_0), reflecting the importance of both commensurability between the pore diameter and bulk period and the imposed curvature in the formation of self-assembled morphologies.

For the case where the pore strongly attract the majority-blocks of the diblock copolymers (case 1), a generic morphological transition sequence, from a string of spheres to a cylinder to helices or stacked toroids is predicted. For larger confining cylindrical pores, this morphological transition sequence repeats in the center of the pore, whereas helices or stacked toroids occur in the outer rings. The predicted sequence of morphological transitions is consistent with the experimental observations in a silica-surfactant composite system confined within cylindrical nanopores in an alumina membrane and SCFT simulations on the model system composed of diblock-copolymer-homopolymer blends of Wu et al.[32] Furthermore, the morphological transition sequence has been confirmed in recent SCFT calculations by Li and Wickham.[30] For the case where the pore is strongly selective to the minority blocks (case 2), the minority blocks are forced to be in contact with the wall. For small pores, the minority blocks form droplets and then a layer at the wall. For larger pores the morphological transition sequence resembles to that of the case of strongly majority-selective walls, with a smaller effective pore diameter. For the case of neutral walls (case 3), the transition sequence of small droplets, rotated droplets, and one layer of helices and then the coaxial two-layer of helices are predicted, besides cylinders parallel and nearly perpendicular to the cylindrical pores. In particular, one layer of helices form when $D/L_0 \approx 1.1$—1.6. This result is in good agreement with the experiments by Xiang et al. on cylinder-forming asymmetric PS-*b*-PBD diblock copolymers confined within cylindrical nanopores in an alumina membrane, where one ring of multiple helices is observed when $D/L_0 \approx 1.1$—1.5.

The chirality of the obtained helical structures has been analyzed based on a large number of independent simulation results for the one-ring structures. It is found that the result is consistent with an equal probability for the left- and right-handed helices. A mechanism of helix formation is proposed based on a packing model for stringlike objects. The radius and the pitch of the observed helical structures are computed. For the case of strongly majority-block selective walls, the radius and pitch angle of the obtained helical structures are compared with theoretical predictions based on the assumption that the helix-forming cylinder has the same diameter as the cylinder in the bulk. Good agreement between the computed value and model predictions is obtained. This agreement indicates that the packing mechanism for the helix formation in our system is reasonable. We also calculated the mean square end-to-end distance of chain and its two components. The mean square end-to-end distance is compared with the bulk values. It is found that the mean square end-to-end distance of chain in all three cases is oscillating with the degree of structural frustration parametrized by the ratio D/L_0. When the effective B-attractive cylindrical pore is considered in case 2, the mean square end-to-end distance of the chains in all three cases exhibits minima when D/L_0 is close to an integer and maxima when D/L_0 is close to a half-integer.

Acknowledgment. We acknowledge useful discussions with Drs. R. A. Wickham and W. Li. This work was supported by the National Natural Science Foundation of China (Grants No. 20474034, No. 20774052, No. 20374031, and No. 20373029), by the Chinese Ministry of Education with the Program of New Century Excellent Talents in Universities (Grant No. ncet-05-0221) and the Program of the Joint-Research Foundation of Nankai and Tianjin Universities, and by Nankai University ISC. ACS gratefully acknowledges the hospitality of St. Francis Xavier University, where the later stages of the manuscript were edited, under a James Chair Visiting Professor Grant, as well as the supports from the Natural Sciences and Engineering Research Council (NSERC) of Canada.

References and Notes

(1) Matsen, M. W.; Schick, M. *Phys. Rev. Lett.* **1994**, *72*, 2660.
(2) Tuzar, Z.; Kratochvil, P. In *Surface and colloid science*; Matijevic, E., Ed.; Plenum Press: New York, 1993; p 15.
(3) Fredrickson, G. H.; Helfand, E. J. *Chem. Phys.* **1987**, *87*, 697.
(4) Hajduk, D. A.; Takenouchi, H.; Hillmyer, M. A.; Bates, F. S.; Vigild, M. E.; Almdal, K. *Macromolecules* **1997**, *30*, 3788.
(5) Russell, T. P. *Curr. Opin. Colloid Interface Sci.* **1996**, *1*, 107.
(6) Bates, F. S.; Fredrickson, G. H. *Annu. Rev. Phys. Chem.* **1990**, *41*, 525.
(7) (a) Boltau, M.; Walheim, S.; Mlynek, J.; Krausch, G.; Steiner, U. *Nature (London)* **1998**, *391*, 877. (b) Boltau, M.; Walheim, S.; Schaffer, E.; Mlynek, J.; Steiner, U. *Science (Washington D.C., U.S.)* **1999**, *283*, 520.
(8) Fink, Y.; Winn, J. N.; Fan, S.; Chen, C.; Michel, J.; Joannopoulos, J. D.; Thomas, E. L. *Science (Washington, D.C.)* **1998**, *282*, 1679.
(9) Bratko, D.; Chakraborty, A. K.; Shakhnovich, E. I. *Phys. Rev. Lett.* **1996**, *76*, 1844.
(10) Kellogg, G. J.; Walton, D. G.; Mayes, A. M.; Lambooy, P.; Russell, T. P.; Gallagher, P. D.; Satija, S. K. *Phys. Rev. Lett.* **1996**, *76*, 2503.
(11) Lambooy, P.; Russell, T. P.; Kellogg, G. J.; Mayes, A. M.; Gallagher, P. D.; Satija, S. K. *Phys. Rev. Lett.* **1994**, *72*, 2899.
(12) Huinink, H. P.; Brokken-Zijp, J. C. M.; van Dijk, M. A.; Sevink, G. J. A. J. *Chem. Phys.* **2000**, *112*, 2452.
(13) Wang, Q.; Nealey, P. F.; de Pablo, J. J. *Macromolecules* **2001**, *34*, 3458.
(14) Knoll, A.; Horvat, A.; Lyakhova, K. S.; Krausch, G.; Sevink, G. J. A.; Zvelindovsky, A. V.; Magerle, R. *Phys. Rev. Lett.* **2002**, *89*, 035501.
(15) Yin, Y.; Sun, P.; Jiang, R.; Li, B.; Chen, T.; Jin, Q.; Ding, D.; Shi, A.-C. *J. Chem. Phys.* **2006**, *124*, 184708.
(16) He, X.; Song, M.; Liang, H.; Pan, C. J. *Chem. Phys.* **2001**, *114*, 10510.
(17) Sevink, G. J. A.; Zvelindovsky, A. V.; Fraaije, J. G. E. M.; Huinink, H. P. J. *Chem. Phys.* **2001**, *115*, 8226.
(18) Chen, P.; He, X.; Liang, H. J. *Chem. Phys.* **2006**, *124*, 104906.
(19) (a) Feng, J.; Ruckenstein, E. *Macromolecules* **2006**, *39*, 4899. (b) Feng, J.; Ruckenstein, E. *J. Chem. Phys.* **2006**, *125*, 164911.
(20) Wang, Q. J. *Chem. Phys.* **2007**, *126*, 024903.
(21) Yu, B.; Sun, P.; Chen, T.; Jin, Q.; Ding, D.; Li, B.; Shi, A.-C. J. *Chem. Phys.* **2007**, *127*, 114906.
(22) Feng, J.; Liu, H. L.; Hu, Y. *Macrom. Theory Simul.* **2006**, *15*, 674.
(23) Xiang, H.; Shin, K.; Kim, T.; Moon, S. I.; McCarthy, T. J.; Russell, T. P. *Macromolecules* **2004**, *37*, 5660.
(24) Shin, K.; Xiang, H.; Moon, S. I.; Kim, T.; McCarthy, T. J.; Russell, T. P. *Science* **2004**, *306*, 76.
(25) A recent review is given in: Xiang, H.; Shin, K.; Kim, T.; Moon, S. I.; McCarthy, T. J.; Russell, T. P. *J. Polym. Sci., B: Polym. Phys.* **2005**, *43*, 3377.
(26) Sun, Y.; Steinhart, M.; Zschech, D.; Adhikari, R.; Michler, G. H.; Goele, U. *Macromol. Rapid Commun.* **2005**, *26*, 369.
(27) Ma, M.; Krikorian, V.; Yu, J. H.; Thomas, E. L.; Rutledge, G. C. *NanoLett.* **2006**, *6*, 2969.
(28) Xiang, H.; Shin, K.; Kim, T.; Moon, S. I.; McCarthy, T. J.; Russell, T. P. *Macromolecules* **2005**, *38*, 1055.
(29) Li, W.; Wickham, R. A.; Garbary, R. A. *Macromolecules* **2006**, *39*, 806.
(30) Li, W.; Wickham, R. A. *Macromolecules* **2006**, *39*, 8492.
(31) Chen, P.; Liang, H.; Shi, A.-C. *Macromolecules* **2007**, *40*, 7329.
(32) Wu, Y.; Cheng, G.; Katsov, K.; Sides, S. W.; Wang, J.; Tang, J.; Fredrickson, G. H.; Moskovits, M.; Stucky, G. D. *Nat. Mater.* **2004**, *3*, 816.
(33) Yu, B.; Sun, P.; Chen, T.; Jin, Q.; Ding, D.; Li, B.; Shi, A.-C. *Phys. Rev. Lett.* **2006**, *96*, 138306.
(34) (a) Kirkpatrick, S.; Gelatt, C. D.; Vecchi, M. P., Jr *Science* **1983**, *220*, 671. (b) Kirkpatrick, S. *J. Stat. Phys.* **1984**, *34*, 975.
(35) Grest, G. S.; Soukoulis, C. M.; Levin, K. *Phys. Rev. Lett.* **1986**, *56*, 1148.
(36) Chakrabarti, A.; Toral, R. *Phys. Rev. B* **1989**, *39*, 542.
(37) Carmesin, I.; Kremer, K. *Macromolecules* **1988**, *21*, 2819.
(38) (a) Larson, R. G. *J. Chem. Phys.* **1992**, *96*, 7904. (b) , *J. Chem. Phys.* **1989**, *91*, 2479.
(39) Yin, Y.; Sun, P.; Chen, T.; Li, B.; Jin, Q.; Ding, D.; Shi, A.-C. *Chem. Phys. Chem.* **2004**, *5*, 540.
(40) Metropolis, N.; Rosenbluth, A. W.; Rosenbluth, M. N.; Teller, A. H.; Teller, E. J. *Chem. Phys.* **1953**, *21*, 1087.
(41) The pitch angle (eq 3) can also be obtained by demanding that the ratio of the projected A-cylinder area to the pore area equals to f_A. Wickham, R. Private communication.

MA702430V